A local metallic state in globally insulating $La_{1.24}Sr_{1.76}Mn_2O_7$ well above the metal–insulator transition

Z. SUN[1,2]*, J. F. DOUGLAS[1], A. V. FEDOROV[2], Y.-D. CHUANG[2], H. ZHENG[3], J. F. MITCHELL[3] AND D. S. DESSAU[1]*

[1]Department of Physics, University of Colorado, Boulder, Colorado 80309, USA
[2]Advanced Light Source, Lawrence Berkeley National Laboratory, Berkeley, California 94720, USA
[3]Materials Science Division, Argonne National Laboratory, Argonne, Illinois 60439, USA
*e-mail: Zhe.Sun@Colorado.edu; Dessau@colorado.edu

Published online: 18 February 2007; doi:10.1038/nphys517

The distinction between metals, semiconductors and insulators depends on the behaviour of the electrons nearest the Fermi level E_F, which separates the occupied from the unoccupied electron energy levels. For a metal, E_F lies in the middle of a band of electronic states, whereas E_F in insulators and semiconductors lies in the gap between states. The temperature-induced transition from a metallic to an insulating state in a solid is generally connected to a vanishing of the low-energy electronic excitations[1]. Here we show the first direct evidence of a counter-example, in which a significant electronic density of states at the Fermi energy exists in the insulating regime. In particular, angle-resolved photoemission data from the colossal magnetoresistive oxide $La_{1.24}Sr_{1.76}Mn_2O_7$ show clear Fermi-edge steps, both below the metal–insulator transition temperature T_C, when the sample is globally metallic, and above T_C, when it is globally insulating. Further, small amounts of metallic spectral weight survive up to temperatures more than twice T_C. Such behaviour may also have close ties to a variety of exotic phenomena in correlated electron systems, including the pseudogap temperature in underdoped cuprates[2].

As shown in Fig. 1a, the colossal magnetoresistive (CMR) oxide $La_{2-2x}Sr_{1+2x}Mn_2O_7$ ($x = 0.36, 0.38$) shows a metal–insulator transition at a T_C just below 130 K, at which point the system also switches from being a ferromagnet (low temperature T) to a paramagnet (high T)[3]. We carried out angle-resolved photoemission spectroscopy (ARPES) experiments on cleaved single crystals of these materials, with an experimental arrangement as described elsewhere[4]. ARPES is an ideal experimental probe of the electronic structure because it gives the momentum-resolved single-particle excitation spectrum. As discussed in ref. 4, the $x = 0.36, 0.38$ compounds studied here do not contain the low-energy pseudogap of the $x = 0.4$ samples[5–8] (see the Methods section for more details on this, the possible issue of surface sensitivity of ARPES and of possible intergrowths at the surface). The much larger metallic spectral weight of these non-pseudogapped compounds also allows us to study the electronic behaviour in greater detail. Although we find only minimal differences between the $x = 0.36$ and $x = 0.38$ compounds, all ARPES spectra shown here are from $x = 0.38$ samples.

Figure 1b shows a large-energy-scale experimental picture of a low-temperature $d_{x^2-y^2}$ symmetry band taken along the blue cut near the zone boundary, as shown in the inset. We are able to get clean data by isolating the various bilayer-split bands using different photon energies, as described in ref. 4. In particular, in this paper we show only data from the antibonding bilayer-split band, which has Fermi crossings at $k_x = \pm 0.17\pi/a$, $k_y = 0.9\pi/a$, corresponding to the solid Fermi surface of the inset of Fig. 1b. The energy-distribution curves (EDCs) at the Fermi wavevector k_F (indicated by the red line in Fig. 1b) taken at a series of temperatures are shown in Fig. 2a. Figure 2b shows the identical spectra and identical scaling, but offset vertically for clarity. All spectra have been normalized only to the incident photon flux.

At low temperature, the EDCs clearly show a peak–dip–hump structure, where the peak and the hump would nominally be considered the coherent part (quasiparticle) and 'incoherent' part of the single-particle spectrum respectively, as has been discussed for the spectra of the high-T_C cuprate superconductors[9–11]. One sees that the near-E_F spectral weight diminishes with increasing temperature, whereas the high-binding-energy (>700 meV) part is less affected by temperature. As will be discussed in future publications, other portions of the Brillouin zone pick up the 'lost' weight from these spectra. Contrary to the general picture of the metal–insulator transition, in which a gap develops in the single-particle spectrum when an electronic system becomes insulating[1], the EDCs here still show a sharp Fermi cutoff, indicating metallic behaviour, at temperatures at which the macroscopic d.c. conductivity is characteristic of insulation (see, for example, the spectra at 135, 150 and 180 K). To our knowledge, this unusual behaviour, a metallic Fermi edge in a globally insulating system, has not been previously observed on the insulating side of a metal–insulator transition. The opposite, in which a metallic system shows a lack of a Fermi cutoff, is on the other hand expected in exotic low-dimensional systems such as the Luttinger liquids[12], and has probably been observed[13]. The other situation most likely to show a metallic Fermi edge in a globally insulating system is that of an Anderson-localized system beyond the mobility edge. However, in such systems a Coulomb gap is expected to remove the metallic weight near the Fermi energy[14]. Our data could be consistent with

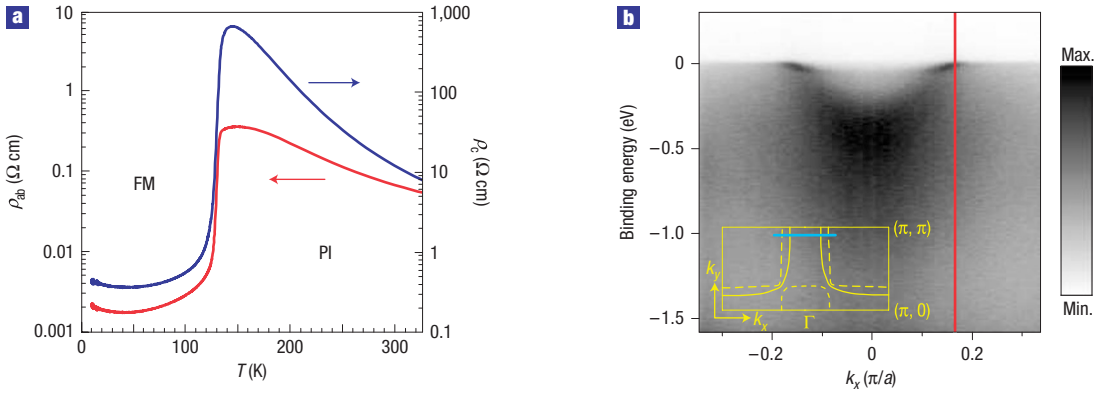

Figure 1 Overview of features of $La_{1.24}Sr_{1.76}Mn_2O_7$ ($x = 0.38$). a, Resistivity versus temperature for a similarly doped ($x = 0.36$) sample, showing a transition between a ferromagnetic metal (FM) and a paramagnetic insulator (PI). Courtesy of K. Gray, Argonne National Laboratory. **b**, Low-temperature (20 K) ARPES data over a large energy scale taken along the blue cut near the zone boundary, as shown in the inset.

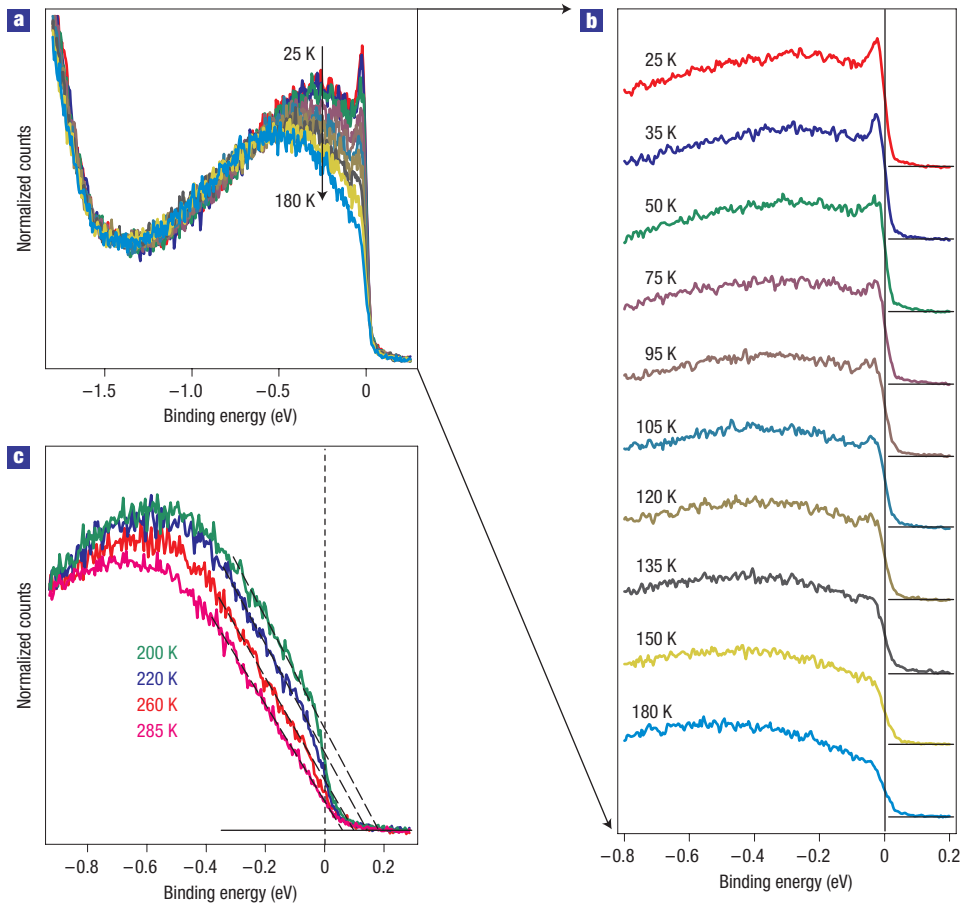

Figure 2 EDCs as a function of temperature at k_F (red line of Fig. 1b), indicating metallic spectral weight above T_c. a,**b**, The same data set scaled by the incident flux and taken while warming. **c**, EDCs from a different sample taken in the high-temperature range. Clear breaks are seen in the spectral intensity near E_F for all but the highest temperature, indicating finite metallic spectral weight and a T^* just above 285 K (see Fig. 3 for details of the T^* determination).

such a scenario only if the Coulomb gap were extremely small—of the order of a few millielectronvolts or less. Moreover, such a picture would not naturally explain the metallic spectral weight dependence on temperature, to be discussed in more detail later.

On a different sample we have carried out higher-temperature scans, looking for a possible temperature scale at which the metallic spectral weight disappears. These data are shown in Fig. 2c and show a clear discontinuity in the slope near the Fermi energy for all

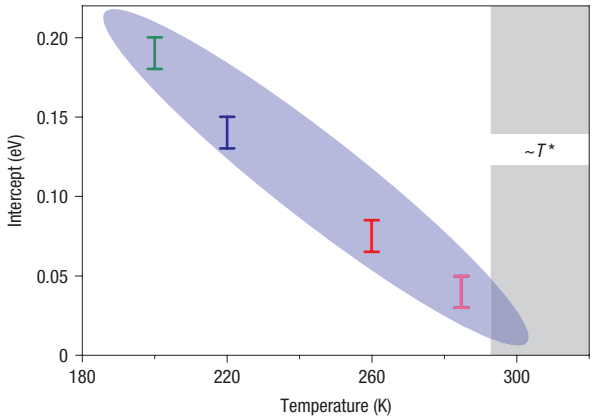

Figure 3 Determination of T^*. The blue-shaded area shows the zero-intensity intercepts in Fig. 2c as a function of temperature. These intercepts go to zero near 300 K (grey shaded area), which we label as T^*. Error bars include uncertainties about the appropriate energy range of Fig. 2c over which to do the linear fits.

but the 285 K data, indicating a finite metallic spectral weight. This effect is emphasized by an extrapolation of the spectral weight using a simple linear fit to the data between −0.3 and −0.05 eV, as shown by the dashed lines in Fig. 2c. On raising the sample temperature we see that the intercept of these dashed lines with the horizontal axis decreases towards zero (E_F) monotonically (Fig. 3). This plot shows that the intercepts should reach zero near 300 K, which should roughly be the temperature where the first bits of metallic weight become apparent. We call this temperature T^*. Technical factors including sample ageing and excessive manipulator drift preclude us from making the full range of measurements on a single cleave. We therefore used different samples to study the electronic excitations in different temperature regimes.

Figure 4a shows the electronic dispersion of the near-Fermi states as a function of temperature obtained from an analysis of momentum-distribution curves (MDCs). These data indicate that the main properties of the metal, such as k_F, the Fermi velocity v_F, the electron–phonon coupling parameter λ and the effective mass m^*, do not change significantly as a function of temperature, even as T_C is traversed. This is unexpected behaviour for a metal–insulator transition, in which these parameters would vary dramatically with temperature, and probably even diverge[1].

Our data can be understood by invoking a model of disconnected local ferromagnetic metallic regimes above T_C up to approximately the temperature T^*. This suggestion is consistent with earlier studies, which have found significant ferromagnetic signals far above T_C (refs 15–18), because metallicity and ferromagnetism should have a connection in these systems via the double-exchange interaction. In general, the metallic regions may be either phase separated (and possibly static) domains[19,20], or they may be dynamic fluctuations of the ferromagnetic metallic state, which in a two-dimensional system may persist to quite high temperatures[15–18]. We will discuss these two possibilities later. Here we show that we can study the metallic portions further by our ability to approximately deconvolve the spectrum into the components that arise from the metal and non-metal portions. We do this by subtracting the 180 K EDC from all other EDCs, as shown in Fig. 2b, to create 'metallic EDCs' or M-EDCs, as shown in Fig. 4b. It should be pointed out that the slight variation of spectra from sample to sample, which has been commonly observed in ARPES, imperils the practice of subtracting data of one sample from those of another. Therefore, we do not use the higher-temperature data of Fig. 2c to carry out the subtraction, as these are from a different sample. Figure 4c shows the same M-EDCs but scaled to all have the same amplitude. Within the noise, all the M-EDCs have similar lineshapes with coherent peaks near E_F and an incoherent background at high binding energy, though the M-EDC coherent peak (or low-energy MDC peak) becomes broader with increasing temperature (Fig. 4d). The integrated spectral weight of the M-EDCs varies smoothly as a function of temperature, with no clear break at T_C (Fig. 4d). This, as well as the approximate temperature independence of the M-EDC lineshape, indicates that the electrons in the metallic regions have similar properties above and below T_C, and that temperature has surprisingly little effect on the behaviour or interactions of electrons in the metallic regions. This is consistent with the approximate independence of v_F, λ and m^* in the metallic regions shown in Fig. 4a. The experimentally determined MDC width of the electrons at the Fermi energy (green triangles of Fig. 4d) does increase with increasing temperature. The inverse of this quantity, the mean free path of the electrons, thus decreases with increasing temperature, consistent with a decreased size of metallic regions or increased scattering events at higher temperatures.

Although many aspects of our data are consistent with either the phase-separation or the magnetic-fluctuation picture, certain aspects of them can address the question of whether the metallic regions above T_C are phase separated out from a more insulating environment[19,20], or whether they are just fluctuations from a lower-temperature ordered environment, which is otherwise homogeneous[17,18]. In particular, the smooth dependence of the spectral weight of the metallic regions as a function of temperature across T_C (blue squares of Fig. 4d) is more consistent with phase separation, as we would expect a clear drop in the metallic weight near T_C if the metallic portions were just fluctuations of the ordered lower-temperature environment. At other doping levels (for example $x = 0.4$), experiments do observe a sharp drop in the metallic weight at T_C to zero or almost zero[8], and so these samples may be more consistent with the fluctuation physics.

Within the picture of phase separation, we imagine that the metallic islands arise at a temperature T^* near room temperature, which may also be related to the temperature scale at which polaronic correlations freeze[21]. As the temperature is lowered the size and proportion of metallic portions grows until a critical ratio of metallic to insulating portions is reached. At this point electrons can percolate from one metallic region to another, bringing about the macroscopic metallic[19] and ferromagnetic states, as well as being consistent with the 'colossal' decrease in resistivity with an applied magnetic field. In certain models this behaviour is expected from a competition between different phases, for example between the ferromagnetic metal phase and the charge-ordered antiferromagnetic insulating phase[19,22,23], though in contrast to ref. 19 the materials used here are far away from the charge-ordered doping level. Theoretical arguments predict both the phase separation and the existence of a higher-temperature scale T^* (ref. 24), with ideas similar to the Griffiths singularity[25], in which T^* would be the critical temperature of the associated clean system in the absence of disorder, and which have recently been discussed in the context of manganite physics[24,26]. We are now undertaking a more thorough study of the full Fermi surface to test this percolation model quantitatively.

A T^* scale is one of the key properties of the high T_C superconductors, and has for years been the subject of intense controversy[2]. In these compounds, disorder also seems to be relevant, especially in the underdoped regime where the T^* scale exists. In this case it signals the emergence of the pseudogap, which may be the precursor to the long-range superconducting order that forms at T_C (ref. 27)—a clear analogy to the manganites, where

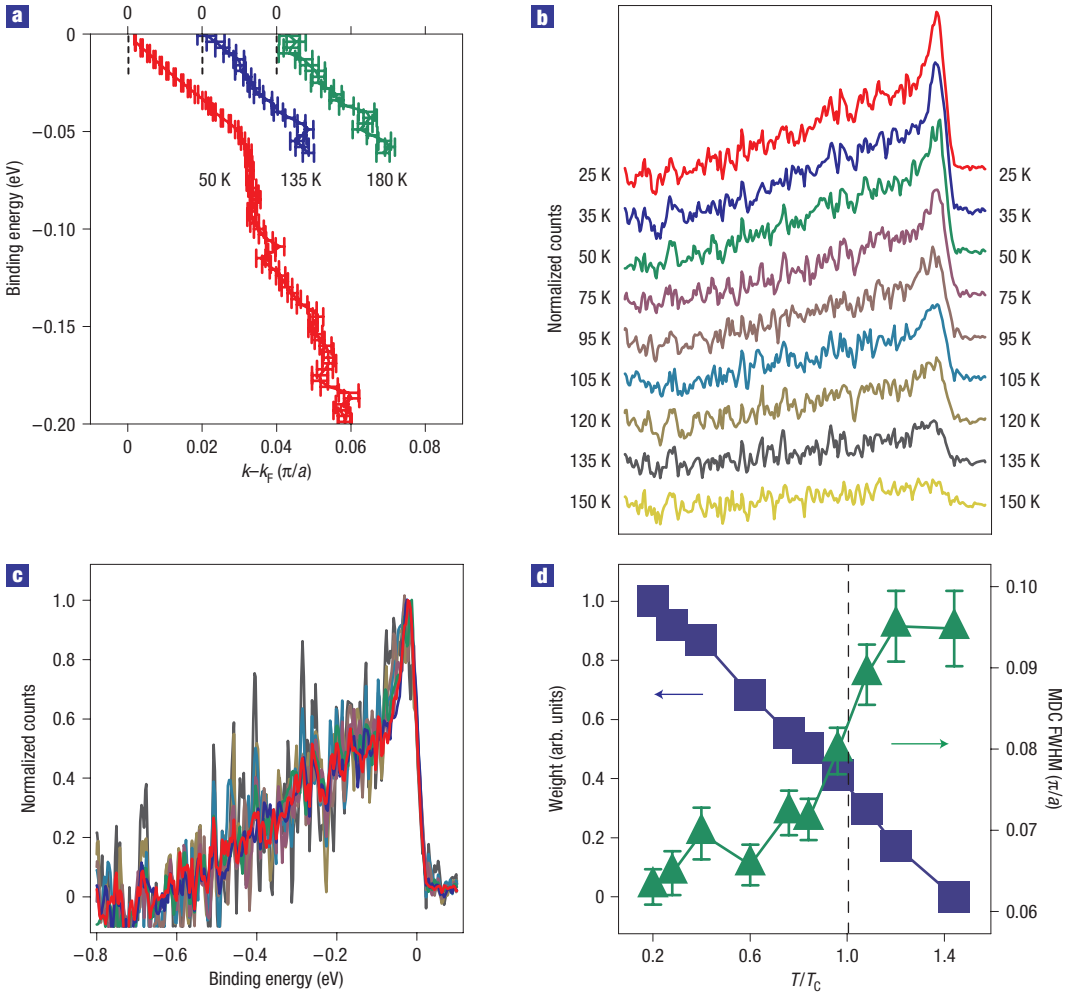

Figure 4 Properties of the metallic portion of the sample. a, Electronic dispersion showing a similar k_F, v_F and λ as a function of temperature. **b**,**c**, Metallic EDCs or M-EDCs obtained by subtracting the 180 K EDC from all lower-temperature data: **b** shows the raw scaling whereas **c** scales each spectrum to have a similar maximum intensity. **d**, MDC widths (green triangles) and integrated M-EDC spectral weights (blue squares) as a function of temperature. The error bars come from the numerical fits of the MDC widths to a lorentzian lineshape.

T^* signals the emergence of the metallic domains, which become long range at T_C. Also similar to the cuprates, it seems that the T^* temperature scales may not be universal to all doping levels of the manganites. Pinning these details down and then understanding their implications will certainly be an area of intense study in the near future.

It is becoming increasingly clear that some of the most dramatic responses in modern materials occur in systems in which multiple phases or orders with similar energy scales compete with each other[22–24,28]. It is then natural that in at least some of these systems spatial heterogeneities will occur, and small perturbations can cause drastic macroscopic alterations to the physical properties or even new types of 'emergent' behaviour. The key is finding out which aspects of the inhomogeneity are intrinsic and what their role is in determining the key physical properties of the system.

METHODS

THE DIFFERENCE BETWEEN $X = 0.38$ AND $X = 0.4$ SAMPLES

It should be pointed out that there is a remarkable difference between the ARPES spectra of $La_{2-2x}Sr_{1+2x}Mn_2O_7$ ($x = 0.38$) and $La_{2-2x}Sr_{1+2x}Mn_2O_7$ ($x = 0.40$) samples, even though many macroscopic properties are similar. Quasiparticles have been found near the zone boundary at the doping levels of $x = 0.36$ and 0.38 in $La_{2-2x}Sr_{1+2x}Mn_2O_7$, although there exists a large energy pseudogap in $x = 0.40$ samples (refs 4–8). Temperature-dependent studies have also been carried out on $x = 0.4$ samples and have not shown any evidence for metallic spectral weight above T_C (refs 6–8). Similar to high-T_C cuprates, physical properties show strong variations with doping in manganites. The cause of the difference between $La_{2-2x}Sr_{1+2x}Mn_2O_7$ ($x = 0.38$) and $La_{2-2x}Sr_{1+2x}Mn_2O_7$ ($x = 0.40$) samples is not understood yet, though it could have to do with the increased lattice anomalies for the 0.4 samples[29], the onset of spin canting between ferromagnetic layers, which starts at the doping level of 0.4 (ref. 30), or even something extrinsic such as a surface issue.

THE ISSUE OF SURFACE SENSITIVITY

Because of the shallow probing depth of the ARPES experiment (~5–10 Å), we cannot completely rule out the potential that a surface phase whose properties do not follow those of the bulk gives rise to some of the phenomena reported here. For ARPES on the layered manganites we are relatively well off because the samples cleave readily between the La,Sr–O bilayers, which are ionically (not covalently) bonded. High-quality low-energy electron diffraction pictures without any evidence of surface reconstruction are obtained from these surfaces. The doping level at the surfaces, as obtained from the Fermi surface

volume, also seems to be correct for these samples—for example the $d_{x^2-y^2}$ bonding-band Fermi surface nesting vector of $0.27 \times (2\pi/a)$ for the $x = 0.38$ samples used in this study[4] exactly matches that obtained from neutron scattering measurements[21]. The nesting vector of 0.4 samples is slightly larger, at $0.3 \times (2\pi/a)$ (ref. 6), and also matches the results of scattering measurements[31].

THE ISSUE OF INTERGROWTHS

One should consider whether it might be possible for the metallic spectral weight far above T_C to have originated from small regions of intergrowth of a higher T_C sample left near the surface after cleaving. Here we discuss why this is inconsistent with our data. Such intergrowths should not arise from a layered manganite, as the maximum temperature at which bulk metallic behaviour is found among all known layered manganites is ~160 K. A small amount of (non-layered) perovskite-like intergrowth with a $T_C = 300$ K could exist at a cleaved surface, though it would not show the bilayer splitting because the perovskite samples have only one MnO_2 plane per unit cell. Both our high- and low-temperature data show this bilayer band splitting (this paper presents only the data from the antibonding component), which is a direct consequence of there being two MnO_2 planes per unit cell. In addition to being able to vary the intensity of the bilayer split bands (relative and overall) by taking advantage of the photoemission matrix elements, we can follow the dispersion in E and k of each of the bilayer bands, including tracking them all the way to E_F. Therefore, we know the origin of the metallic weight as explicitly originating from these bilayer split bands, and therefore from the bilayer manganite.

Received 6 October 2006; accepted 19 December 2006; published 18 February 2007.

References

1. Imada, M., Fujimori, A. & Tokura, Y. *et al.* Metal–insulator transitions. *Rev. Mod. Phys.* **70**, 1039–1263 (1998).
2. Timusk, T. & Statt, B. The pseudogap in high-temperature superconductors: An experimental survey. *Rep. Prog. Phys.* **62**, 61–122 (1999).
3. Li, Q. A., Gray, K. E. & Mitchell, J. F. Spin-independent and spin-dependent conductance anisotropy in layered colossal-magnetoresistive manganite single crystals. *Phys. Rev. B* **59**, 9357–9361 (1999).
4. Sun, Z. *et al.* Quasiparticlelike peaks, kinks, and electron-phonon coupling at the $(\pi, 0)$ regions in the CMR oxide $La_{2-2x}Sr_{1+2x}Mn_2O_7$. *Phys. Rev. Lett.* **97**, 056401 (2006).
5. Dessau, D. S. *et al.* k-dependent electronic structure, a large "ghost" Fermi surface, and a pseudogap in a layered magnetoresistive oxide. *Phys. Rev. Lett.* **81**, 192–195 (1998).
6. Chuang, Y.-D. *et al.* Fermi surface nesting and nanoscale fluctuating charge/orbital ordering in colossal magnetoresistive oxides. *Science* **292**, 1509–1513 (2001).
7. Saitoh, T. *et al.* Temperature-dependent pseudogaps in colossal magnetoresistive oxides. *Phys. Rev. B* **62**, 1039–1043 (2000).
8. Mannella, N. *et al.* Nodal quasiparticle in pseudogapped colossal magnetoresistive manganites. *Nature* **438**, 474–478 (2005).
9. Dessau, D. S. *et al.* Anomalous spectral weight transfer at the superconducting transition of $Bi_2Sr_2CaCu_2O_{8+\delta}$. *Phys. Rev. Lett.* **66**, 2160–2163 (1991).
10. Shen, Z.-X. & Dessau, D. S. Electronic structure and photoemission studies of late transition-metal oxides—Mott insulators and high-temperature superconductors. *Phys. Rep.* **253**, 1–162 (1995).
11. Damascelli, A., Hussain, Z. & Shen, Z.-X. Angle-resolved photoemission studies of the cuprate superconductors. *Rev. Mod. Phys.* **75**, 473–541 (2003).
12. Voit, J. One-dimensional Fermi liquids. *Rep. Prog. Phys.* **57**, 977–1116 (1995).
13. Allen, J. W. Quasiparticles and their absence in photoemission spectroscopy. *Solid State Commun.* **123**, 469–487 (2002).
14. Varma, C. M. Electronic and magnetic states in the giant magnetoresistive compounds. *Phys. Rev. B* **54**, 7328–7333 (1996).
15. Argyriou, D. N. *et al.* Two-dimensional ferromagnetic correlations above T_C in the naturally layered CMR manganite $La_{2-2x}Sr_{1+2x}Mn_2O_7$ ($x = 0.3$–0.4). *J. Appl. Phys.* **83**, 6374–6378 (1998).
16. Osborn, R. *et al.* Neutron scattering investigation of magnetic bilayer correlations in $La_{1.2}Sr_{1.8}Mn_2O_7$: Evidence of canting above T_C. *Phys. Rev. Lett.* **81**, 3964 (1998).
17. Rosenkranz, S. *et al.* Observation of Kosterlitz–Thouless spin correlations in the colossally magnetoresistive layered manganite $La_{1.2}Sr_{1.8}Mn_2O_7$. Preprint at <http://www.arxiv.org/abs/cond-mat/9909059> (1999).
18. Rosenkranz, S. *et al.* Spin correlations and magnetoresistance in the bilayer manganite $La_{1.2}Sr_{1.8}Mn_2O_7$. *Physica B* **312–313**, 763–765 (2002).
19. Uehara, M., Mori, S., Chen, C. H. & Cheong, S.-W. Percolative phase separation underlies colossal magnetoresistance in mixed-valent manganites. *Nature* **399**, 560–563 (1999).
20. Dagotto, E. *Nanoscale Phase Separation and Colossal Magnetoresistance: The Physics of Manganites and Related Compounds* (Springer, Berlin, 2003).
21. Argyriou, D. N. *et al.* Glass transition in the polaron dynamics of colossal magnetoresistive manganites. *Phys. Rev. Lett.* **89**, 36401 (2002).
22. Dagotto, E. Complexity in strongly correlated electronic systems. *Science* **309**, 257–262 (2005).
23. Tokura, Y. Critical features of colossal magnetoresistive manganites. *Rep. Prog. Phys.* **69**, 797–851 (2006).
24. Burgy, J., Mayr, M., Martin-Mayor, V., Moreo, A. & Dagotto, E. Colossal effects in transition metal oxides caused by intrinsic inhomogeneities. *Phys. Rev. Lett.* **87**, 277202 (2001).
25. Griffiths, R. B. Nonanalytic behavior above the critical point in a random Ising ferromagnet. *Phys. Rev. Lett.* **23**, 17 (1969).
26. Salamon, M. B., Lin, P. & Chun, S. H. Colossal magnetoresistance is a Griffiths singularity. *Phys. Rev. Lett.* **88**, 197203 (2002).
27. Emery, V. J. & Kivelson, S. A. Importance of phase fluctuations in superconductors with small superfluid density. *Nature* **374**, 434–437 (1995).
28. Murakami, S. & Nagaosa, N. Colossal magnetoresistance in manganites as a multicritical phenomenon. *Phys. Rev. Lett.* **90**, 197201 (2003).
29. Mitchell, J. *et al.* Spin, charge and lattice states in layered magneto-resistive oxides. *J. Phys. Chem. B* **105**, 10731–10745 (2001).
30. Kubota, M. *et al.* Relation between crystal and magnetic structures of layered maganite $La_{2-2x}Sr_{1+2x}Mn_2O_7$ ($0.30 \le x \le 0.50$). *J. Phys. Soc. Jpn* **69**, 1606–1609 (2000).
31. Vasiliu-Doloc, L. *et al.* Charge melting and polaron collapse in $La_{1.2}Sr_{1.8}Mn_2O_7$. *Phys. Rev. Lett.* **83**, 4393–4396 (1999).

Acknowledgements

The authors thank K. Gray for the resistivity data of Fig. 1a and Y. Tokura and T. Kimura for providing preliminary samples, and are grateful to D. N. Argyriou, A. Bansil, E. Dagotto, K. Gray, A. Moreo, R. Osborn, L. Radzihovsky, D. Reznik, S. Rosenkranz, Y. Tokura and M. Veillette for helpful discussions. Primary support for this work came from US National Science Foundation grant DMR 0402814, with other support from the US Department of Energy under grant DE-FG02-03ER46066. The Advanced Light Source is supported by the Director, Office of Science, Office of Basic Energy Sciences, US Department of Energy, under contract No. DE-AC02-05CH11231. Argonne National Laboratory, a US Department of Energy Office of Science Laboratory, is operated under contract No. DE-AC02-06CH11357. The US Government retains for itself, and others acting on its behalf, a paid-up non-exclusive, irrevocable worldwide license in said article to reproduce, prepare derivative works, distribute copies to the public and perform publicly and display publicly, by or on behalf of the government.
Correspondence and requests for materials should be addressed to D.S.D. or Z.S.

Competing financial interests

The authors declare no competing financial interests.